11th International Symposium on Turbulence and Shear Flow Phenomena (TSFP11)
Southampton, UK, July 30 to August 2, 2019

A NOVEL IMPROVEMENT OF COMPACT NONLINEAR SCHEME FOR SIMULATING COMPRESSIBLE FLOWS

Huaibao Zhang
School of Physics
Sun Yat-sen University
Guangzhou 510006, Guangdong, China
zhanghb28@mail.sysu.edu.cn
huaibao.zhang@gmail.com

Fan Zhang
School of Aeronautics and Astronautics
Sun Yat-sen University
Guangzhou 510006, Guangdong, China
zhangfan.zf@mail.ru

Guangxue Wang
School of Physics
Sun Yat-sen University
Guangzhou 510006, Guangdong, China

Chunguang Xu
School of Aeronautics and Astronautics
Sun Yat-sen University
Guangzhou 510006, Guangdong, China

Abstract

Weighted compact nonlinear schemes (WCNSs) were developed to improve the performance of compact high-order nonlinear schemes (CNSs) by utilizing the weighting technique originally designed for WENO schemes, and non-oscillatory shock-capturing computation and high resolution in smooth flow field are both achieved. Extensive efforts have been given focusing on improving the performance of WCNSs ever since then. In this work, the ENO-like stencil selection procedure of TENO schemes is introduced for high-order nonlinear interpolations of midpoint variables, targeting compact nonlinear schemes which fully abandon the oscillatory stencils crossing discontinuities and eliminate numerical oscillations. The stencil selection procedure also directly applies smooth stencils with their optimal weights, ensuring that the optimal numerical accuracy is fully recovered in smooth flow field.

1 Introduction

While second-order accurate numerical methods along with RANS simulations are frequently implemented by commercial codes, and currently dominate most industry related applications, high-order CFD schemes are still expected candidates when much of the attention is given on problems containing both discontinuities and complex flow structures, such as shock-boundary layer interaction, Rayleigh-Taylor instability, and particularly the numerical simulation of compressible turbulence flows. However, high-resolution simulations of compressible flows containing discontinuities are still challenging even for current state-of-the-art numerical methods. Therefore, the development of advanced high-order CFD schemes, targeting non-oscillatory computation for shock-capturing and high-order accuracy in smooth flow field, is still an active topic with much to be done.

Compact finite difference schemes have displayed spectral-like resolution Lele (1992), which are therefore highly favored in the simulation of flow problems involving multi-scales phenomena. Weighted Compact Nonlinear Schemes (WCNSs) Deng & Zhang (2000) are a family of high resolution nonlinear shock-capturing schemes developed based on the key concept of nonlinear weighting technique and cell-centered compact schemes. Past research has been performed on WCNSs, notably by Nonomura *et al.* (2010); Nonomura & Fujii (2013); Wong & Lele (2017), demonstrating that WCNSs have several advantages over the standard finite-difference Weighted Essentially Non-oscillatory (WENO) schemes Liu *et al.* (1994): (1) the resolution is slightly higher; (2) the choice of flux schemes is more flexible, including Roe scheme Roe (1981), van Leer scheme van Leer (1982), and AUSM scheme Liou (1993); and (3) WCNS performs well on freestream and vortex preservation properties on wavy grids.

The classical WCNS procedure consists of three steps Deng & Zhang (2000): (1) the node-to-midpoint weighted nonlinear interpolation of flow variables, (2) the evaluation of fluxes at midpoints, and (3) midpoint-to-node central flux differencing. The flux differencing in the third step can be performed by using compact schemes or explicit schemes. Despite that a compact scheme is used by the classical WCNS, later work of Deng *et al.* (2005) suggested that for a fourth or fifth-order WCNS, the weighted nonlinear interpolation in step (1) dominates the resolution property, and explicit central differencing scheme is recommended due to its simplicity of implementation and superior computation efficiency. Further work of Nonomura & Fujii (2009) demonstrated that the type of flux differencing does not significantly change the resolution, even for higher-order WCNSs. The classical WCNS uses the strategy by Jiang & Shu (1996), and is therefore referred to as WCNS-JS.

Recently, a family of high-order targeted ENO schemes has been proposed by Fu *et al.* (2016). One of the essential feature of the TENO scheme is the use of ENO-type stencil selection procedure. Instead of merely focusing on developing improved nonlinear weights, the stencil selection technique is incorporated in WCNS, and the so-called fifth-order TCNS is developed in this work. In Section 2 we specifically discuss numerical methods being used. Numerical results of canonical test cases, as well as the corresponding discussion, are given in section 3. Finally, concluding remarks are given in the last section.

2 Numerical methods

Without loss of generality, the one-dimensional scalar hyperbolic conservation law

$$\frac{\partial u}{\partial t}+\frac{\partial f(u)}{\partial x}=0, \tag{1}$$

which is subject to the initial condition

$$u(x,0)=u_0(x), \tag{2}$$

is used to explain the numerical methods which are eventually implemented to solve the governing equations of compressible flows.

The spatial discretization of Eq. (1) is performed on an equally spaced one-dimensional mesh. The distance between two adjacent grid nodes is h. An ordinary differential equation (ODE) system is obtained

$$\frac{du_i}{dt}=-\frac{\partial f}{\partial x}|_{x=x_i}=-f_i', \quad i=1,\cdots,n. \tag{3}$$

As mentioned above, the first-order derivative of the flux function, i.e. f_i', can be approximated by using implicit or explicit central differencing schemes. Here, an explicit midpoint-to-node central differencing scheme is used to calculate the flux derivatives at grid nodes, given by

$$f_i'=\frac{75}{64h}(\hat{f}_{i+\frac{1}{2}}-\hat{f}_{i-\frac{1}{2}})-\frac{25}{384h}(\hat{f}_{i+\frac{3}{2}}-\hat{f}_{i-\frac{3}{2}})+\frac{3}{640h}(\hat{f}_{i+\frac{5}{2}}-\hat{f}_{i-\frac{5}{2}}). \tag{4}$$

Midpoint flux terms in Eq.(4) are unknown and can be evaluated using numerical upwind flux functions. The scalar upwind flux function can be written in a generic form

$$\hat{f}_{i\pm\frac{1}{2}}=\frac{1}{2}\left[\left(f(u_{R,i\pm\frac{1}{2}})+f(u_{L,i\pm\frac{1}{2}})\right)-|\hat{a}|\left(u_{R,i\pm\frac{1}{2}}-u_{L,i\pm\frac{1}{2}}\right)\right], \tag{5}$$

where the subscripts, L and R, respectively indicate the variables on the left and right hand side of midpoint $x_{i\pm\frac{1}{2}}$, and $\hat{a}$ is the approximate eigenvalue.

2.1 High-order nonlinear interpolation of midpoint variables

Following the work of WCNS, the high-order nonlinear interpolation procedure is applied on the midpoint flow variable $u_{L/R,i\pm\frac{1}{2}}$. For the purpose of simplicity, we only focus on the evaluation of variable on the left hand side of $x_{i+\frac{1}{2}}$, i.e., $u_{L,i+\frac{1}{2}}$, in the following work. The evaluation of $u_{R,i+\frac{1}{2}}$ can be performed straightforwardly by using a symmetrical form of $u_{L,i+\frac{1}{2}}$.

The fifth-order accurate linear approximation of the midpoint variable $u_{L,i+\frac{1}{2}}$ takes the form of

$$u_{L,i+\frac{1}{2}}=u_i+\frac{1}{128}\left(3u_{i-2}-20u_{i-1}-38u_i+60u_{i+1}-5u_{i+2}\right), \tag{6}$$

which is constructed by employing a five-point full stencil $S_{i+\frac{1}{2}}=\{x_{i-2},x_{i-1},x_i,x_{i+1},x_{i+2}\}$.

Eq. (6), however, can be equivalently represented by combining three third-order polynomials each constructed on the following three-point substencil

$$S_{i+\frac{1}{2},k}=\{x_{i+k-2},x_{i+k-1},x_{i+k}\}, \quad k=0,1,2, \tag{7}$$

which is shown in Fig. 1.

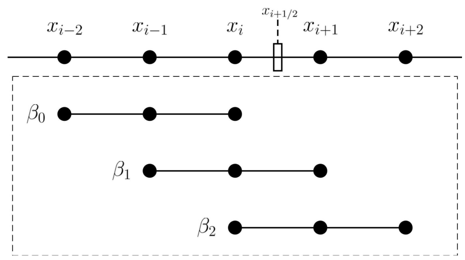

Figure 1. Stencils for the fifth-order interpolation

Each of the third-order polynomials can be expressed in a generic form using the (approximated) $n-$th derivatives $(n=1,2)$

$$u_{L,i+\frac{1}{2},k}=u_i\left(x_i+\Delta x\right)=u_i+u_{i,k}^{(1)}\Delta x+u_{i,k}^{(2)}\frac{\Delta x^2}{2}, \tag{8}$$

where $\Delta x=x_{i+\frac{1}{2}}-x_i=\frac{h}{2}$. The first- and second-order derivatives are respectively given by

$$\begin{aligned}
u_{i,0}^{(1)}&=\frac{1}{2h}(u_{i-2}-4u_{i-1}+3u_i),\\
u_{i,1}^{(1)}&=\frac{1}{2h}(u_{i+1}-u_{i-1}),\\
u_{i,2}^{(1)}&=\frac{1}{2h}(-3u_i+4u_{i+1}-u_{i+2}),
\end{aligned} \tag{9}$$

and

$$\begin{aligned}
u_{i,0}^{(2)}&=\frac{1}{h^2}(u_{i-2}-2u_{i-1}+u_i),\\
u_{i,1}^{(2)}&=\frac{1}{h^2}(u_{i-1}-2u_i+u_{i+1}),\\
u_{i,2}^{(2)}&=\frac{1}{h^2}(u_i-2u_{i+1}+u_{i+2}).
\end{aligned} \tag{10}$$

The linear optimal scheme is then represented by

$$u_{L,i+\frac{1}{2}}=\sum_{k=0}^{2}d_k u_{L,i+\frac{1}{2},k}, \tag{11}$$

where the optimal linear weights are

$$d_0=\frac{1}{16}, \quad d_1=\frac{10}{16}, \quad d_2=\frac{5}{16}. \tag{12}$$

Nonlinear weights are used to take the place of optimal linear weights in order to alleviate non-physical oscillations when candidate substencils cross discontinuities. For instance, the nonlinear weights of Jiang & Shu (1996) are given by

$$\omega_k = \frac{\alpha_k}{\sum_{k=0}^{2} \alpha_k}, \quad \alpha_k = \frac{d_k}{(\beta_k + \varepsilon)^2}, \tag{13}$$

where the small parameter $\varepsilon = 10^{-6}$ is used to prevent division by zero, and β_k is the local smoothness indicator in the form of

$$\beta_k = \left(h u_{i,k}^{(1)}\right)^2 + \left(h^2 u_{i,k}^{(2)}\right)^2. \tag{14}$$

It can be readily found that the corresponding JS weight can adaptively approach 0 for a candidate substencil crossed by discontinuities, diminishing possible numerical oscillations, and continuously approximate the optimal linear weight in smooth regions, therefore achieving high-order accuracy.

2.2 ENO-type stencil-selection

Instead of merely concentrating on improving nonlinear weights, the ENO-like stencil-selection procedure Fu *et al.* (2016) is introduced in this work as an essential component of the presented method. In particular, the nonlinear smoothness measurement yielding strong scale-separation mechanism is given by

$$\gamma_k = \left(C + \frac{\tau_5}{\beta_k + \varepsilon}\right)^q, \quad k = 0, 1, 2, \tag{15}$$

where $\tau_5 = |\beta_0 - \beta_2|$ is the global smoothness indicator which was originally proposed in the reference of Borges *et al.* (2008), and the small threshold is given by $\varepsilon = 10^{-40}$, following that of WENO-Z scheme Borges *et al.* (2008) as well. Constant $C = 1$ is set, and the integer power $q = 6$ is used.

Instead of directly using the nonlinear smoothness measurement of γ_k in Eq. (15), it is further normalized by

$$\chi_k = \frac{\gamma_k}{\sum_{k=0}^{2} \gamma_k}, \tag{16}$$

which is then subject to a sharp cut-off function

$$\delta_k = \begin{cases} 0, \text{ if} & \chi_k < C_T, \\ 1, & \text{otherwise.} \end{cases} \tag{17}$$

By introducing a parameter C_T as the threshold of the cut-off procedure, each candidate stencil can be attributed as "smooth" or "oscillatory", such that those genuinely oscillatory stencils are abandoned thereby, and only smooth ones are used with their corresponding optimal linear weights in the final interpolation. Observation of Eq. (17) indicates that using a smaller C_T tends to better recover the underlying linear scheme, and yields better spectral properties.

Table 1. The coefficients of seven possible resulting polynomials for the high-order nonlinear interpolation.

$\delta_{0,1,2}$	$\hat{u}^*_{L,i+\frac{1}{2},m}$	S^*_m	$a_{m,i-2}$	$a_{m,i-1}$	$a_{m,i}$	$a_{m,i+1}$	$a_{m,i+2}$
1,1,1	$\hat{u}^*_{L,i+\frac{1}{2},0}$	S^*_0	3/128	-5/32	45/64	15/32	-5/128
0,1,1	$\hat{u}^*_{L,i+\frac{1}{2},1}$	S^*_1	0	-1/12	5/8	1/2	-1/24
1,1,0	$\hat{u}^*_{L,i+\frac{1}{2},2}$	S^*_2	3/88	-5/22	75/88	15/44	0
0,0,1	$\hat{u}^*_{L,i+\frac{1}{2},3}$	S^*_3	0	0	3/8	3/4	-1/8
0,1,0	$\hat{u}^*_{L,i+\frac{1}{2},4}$	S^*_4	0	-1/8	3/4	3/8	0
1,0,0	$\hat{u}^*_{L,i+\frac{1}{2},5}$	S^*_5	3/8	-5/4	15/8	0	0
1,0,1	$\hat{u}^*_{L,i+\frac{1}{2},6}$	S^*_6	1/16	-5/24	5/8	5/8	-5/48

The resulting weight functions are finally given by

$$\omega_k^{(T)} = \frac{d_k \delta_k}{\sum_{k=0}^{2} d_k \delta_k}, \tag{18}$$

where the cut-off function δ_k in Eq. (17) is incorporated into the weight evaluation to switch on/off each candidate substencil. Different from the continuously varying nonlinear weight of JS in Eq. (13), the new weight in Eq. (18) in fact belongs to a set of several numbers (this set has seven elements as will be shown in the following paragraphs), since only two possible values of $d_k \delta_k$ exist, viz., d_k and 0.

After applying this weighting strategy along with the cut-off procedure, the number of possible convex combinations of candidate stencils is seven, represented in a generic form

$$\hat{u}^*_{L,i+\frac{1}{2},m} = \sum_{l=i-2}^{i+2} a_{m,l} u_l, \tag{19}$$

where the coefficients are shown in Table 1. As a comparison, the number of possible convex combinations is infinite when using the JS weight. Each combination of three substencils, as shown in Table 1, leads to a high-order interpolation for the midpoint variables.

3 Numerical results and discussions

A variety of canonical problems are simulated to assess the performance of the proposed fifth-order scheme TCNS, compared against WCNS-JS. One-dimensional linear advection equation and Euler equations of gas dynamics are used as model equations. The ideal-gas equation of state is given by $p = (\gamma - 1)\rho e$ with $\gamma = 1.4$ to close the Euler equations. The node-to-midpoint interpolation is performed on characteristic variables to alleviate spurious oscillations Deng & Zhang (2000). The van leer scheme van Leer (1982) is used for the computation of numerical fluxes. We note that a CFL number equal to 0.6 has been used as default for all numerical schemes and test cases reported herein.

3.1 Approximate dispersion relation

The ADR analysis introduced by Pirozzoli (2006) is performed to evaluate the spectral properties of the numerical schemes, and notes of Mao *et al.* (2015) are followed to proceed the numerical procedure of ADR, e.g. the setup of the time step size. As shown in Fig. 2(a) and 2(b), the solutions obtained by the proposed TCNS agree well with the underlying linear scheme in low and intermediate wavenumbers. A significant improvement can be found when compared against the WCNS-JS in both dispersion and dissipation properties. In addition, three numerical solutions of varying threshold C_Ts for TCNS are also presented to show the effect of threshold C_T on dispersion and dissipation properties. Using small threshold C_T delays the separation from the results of the underlying linear scheme, indicating relatively superior spectral properties. However, the threshold $C_T = 10^{-5}$ is used as a compromise of both decent spectral properties and numerical robustness for shock-capturing.

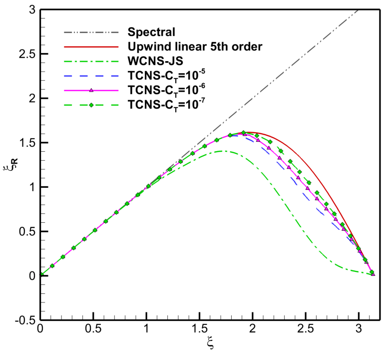

(a) Dispersion

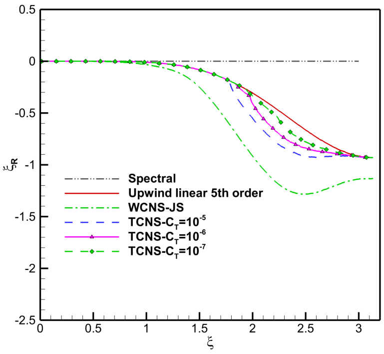

(b) Dissipation

Figure 2. Approximated dispersion and dissipation properties of fifth-order schemes.

3.2 Linear advection problem

The Gaussian pulse advection problem in one-dimension Yamaleev & Carpenter (2009) is used to assess the numerical order of accuracy of the proposed scheme. This problem is modeled by the linear advection equation, with periodic boundary conditions and the initial conditions given by

$$u(x,0) = e^{-300(x-x_c)^2}, \quad x_c = 0.5. \tag{20}$$

Time integration is performed up to $t = 1$, which corresponds to one period of the single wave propagation in time. A set of evenly distributed grids are progressively refined by a factor of 2 from the most coarse grid of 51 points. The numerical simulation on each grid is conducted using sufficiently small time steps to archive temporally converged results.

Table 2 illustrates the numerical errors and convergence rates of all fifth-order numerical schemes. The result of TCNS coincides with that of the underlying linear scheme. WCNS-JS also shows approximate fifth-order accuracy, but its resolution is significantly lower than that of TCNS. In general, using the ENO-like stencil-selection procedure recovers the optimal linear scheme in this smooth field.

Table 2. L_∞-error and convergence rate of different fifth-order schemes solving the linear advection equation.

N	Linear		WCNS-JS		TCNS	
	Error	Order	Error	Order	Error	Order
51	5.22E-02	*	1.07E-01	*	5.20E-02	*
101	3.30E-03	3.98	1.04E-02	3.37	3.30E-03	3.98
201	1.16E-04	4.83	4.63E-04	4.49	1.16E-04	4.83
401	3.69E-06	4.97	1.84E-05	4.66	3.69E-06	4.97
801	1.16E-07	4.99	6.36E-07	4.85	1.16E-07	4.99
1601	3.64E-09	4.99	2.02E-08	4.98	3.64E-09	4.99

3.3 Shock-density wave interaction

The shock-density wave interaction problem Shu & Osher (1989) is characterized by a right moving Mach 3 shock interacting with sine waves in the density field. The multi-scale wave structure is evolved after the shock wave interacts with the oscillating density wave, and both the shock-capturing and wave-resolving capabilities are evaluated thereafter.

The problem is governed by Euler equations and initialized by

$$(\rho, u, p) = \begin{cases} (3.857, 2.629, 10.333), & x \in [0,1], \\ (1+0.2\sin(5x), 0, 1), & x \in (1,10]. \end{cases} \tag{21}$$

This case is run on a grid of $N = 201$ points which are uniformly distributed and the final time is $t = 1.8$. Numerical solution of WCNS-JS on a grid of $N = 2001$ is used as the reference "exact" solution.

As shown in Fig. 3, TCNS produces considerably better resolved density waves behind the shock wave compared with WCNS-JS. Particularly, the result of WCNS-JS indicates strong numerical dissipation, since the small-scale wave structures are relatively smeared.

3.4 Rayleigh-Taylor instability

Rayleigh-Taylor instability problem is used to examine the performance of the presented method. Two sets of grids are used with the resolutions of 128×512 and 256×1024, respectively. The initial conditions are given by

$$(\rho, u, v, p) = \begin{cases} (2, 0, -0.025a\cos(8\pi x), 1+2y) & x \in [0, 0.25] \text{ and } y \in [0, 0.5), \\ (1, 0, -0.025a\cos(8\pi x), 1+3/2) & x \in [0, 0.25] \text{ and } y \in [0.5, 1], \end{cases} \tag{22}$$

where a is the speed of sound, given by $a = \sqrt{\gamma \frac{p}{\rho}}$ and a different $\gamma = \frac{5}{3}$ is used for this specific case. Reflecting boundary conditions are imposed at the left and right side of the domain, and constant boundary conditions are given for the top and the bottom sides, in details

$$(\rho,u,v,p) = \begin{cases} (1,0,0,2.5) & y=1, \quad \forall t,x, \\ (2,0,0,1) & y=0, \quad \forall t,x. \end{cases} \tag{23}$$

Two source terms ρ, and ρv are added to the right hand side of the third and the fourth equation, respectively.

Density profiles at $t = 1.95$ are shown in Fig.4. It can be found that the presented scheme captures much more abundant wave structures compared with WCNS-JS. Moreover, TCNS on a coarse grid achieves similar or even better result compared with WCNS-JS on a fine grid.

4 Conclusions

A novel compact nonlinear scheme, which applies the ENO-like stencil-selection procedure, is introduced in this article. This method named as TCNS aims at achieving the optimal linear interpolation in the node-to-midpoint interpolation step of the compact nonlinear scheme. The ADR analysis shows that TCNS recovers the underlying linear scheme up to high wave numbers, even using a relative large cut-off threshold. It is also demonstrated by using the linear advection case that TCNS is capable of fully recovering the underlying optimal linear scheme in a smooth flow field, by directly applying the optimal linear weights in the node-to-midpoint interpolation procedure. Moreover, significant improvements are obtained by TCNS in numerical tests such as the shock-density wave interaction problem and the Rayleigh-Taylor instability case, which are characterized by broadband fluctuations and rich small scales, respectively. These significant improvements of TCNS are mostly attributed to the use of the ENO-like stencil-selection procedure, which yields considerably low dissipation and dispersion errors compared against WCNS-JS.

REFERENCES

Borges, Rafael, Carmona, Monique, Costa, Bruno & Don, Wai Sun 2008 An improved weighted essentially non-oscillatory scheme for hyperbolic conservation laws. *Journal of Computational Physics* **227** (6), 3191–3211.

Deng, X., Liu, X., Mao, M. & Zhang, H. 2005 Investigation on weighted compact fifth-order nonlinear scheme and applications to complex flow. In *17th AIAA Computational Fluid Dynamics Conference*. Toronto, Ontario Canada: AIAA Paper 2005-5246.

Deng, Xiaogang & Zhang, Hanxin 2000 Developing high-order weighted compact nonlinear schemes. *Journal of Computational Physics* **165** (1), 22 – 44.

Fu, Lin, Hu, Xiangyu Y. & Adams, Nikolaus A. 2016 A family of high-order targeted ENO schemes for compressible-fluid simulations. *Journal of Computational Physics* **305**, 333–359.

Jiang, Guang-Shan & Shu, Chi-Wang 1996 Efficient implementation of weighted ENO schemes. *Journal of Computational Physics* **126** (1), 202–228.

van Leer, Bram 1982 Flux-vector splitting for the Euler equations. In *Eighth International Conference on Numerical Methods in Fluid Dynamics* (ed. E. Krause), *Lecture Notes in Physics*, vol. 170, pp. 507–512. Aachen, Germany: Springer Berlin Heidelberg.

Lele, Sanjiva K. 1992 Compact finite difference schemes with spectral-like resolution. *Journal of Computational Physics* **103** (1), 16 – 42.

Liou, M. S. 1993 On a new class of flux splittings. In *Thirteenth International Conference on Numerical Methods in Fluid Dynamics* (ed. M. Napolitano & F. Sabetta), *Lecture Notes in Physics*, vol. 414, pp. 115–119. Berlin, Heidelberg: Springer Berlin Heidelberg.

Liu, Xu Dong, Osher, Stanley & Chan, Tony 1994 Weighted essentially non-oscillatory schemes. *Journal of Computational Physics* **115** (1), 200–212.

Mao, Meiliang, Yan, Zhenguo, Liu, Huayong, Zhu, Huajun & Deng, Xiaogang 2015 Study of quasi-linear spectral analysis method of high-order weighted nonlinear schemes. *Acta Aerodynamica Sinica* **33** (1), 1–9.

Nonomura, Taku & Fujii, Kozo 2009 Effects of difference scheme type in high-order weighted compact nonlinear schemes. *Journal of Computational Physics* **228** (10), 3533 – 3539.

Nonomura, Taku & Fujii, Kozo 2013 Robust explicit formulation of weighted compact nonlinear scheme. *Computers & Fluids* **85**, 8 – 18, international Workshop on Future of CFD and Aerospace Sciences.

Nonomura, Taku, Iizuka, Nobuyuki & Fujii, Kozo 2010 Freestream and vortex preservation properties of high-order weno and wcns on curvilinear grids. *Computers & Fluids* **39** (2), 197 – 214.

Pirozzoli, Sergio 2006 On the spectral properties of shock-capturing schemes. *Journal of Computational Physics* **219** (2), 489 – 497.

Roe, Philip L 1981 Approximate Riemann solvers, parameter vectors, and difference schemes. *Journal of Computational Physics* **43** (2), 357–372.

Shu, Chi-Wang & Osher, Stanley 1989 Efficient implementation of essentially non-oscillatory shock-capturing schemes,ii. *J. Comput. Phys.* **83** (1), 32–78.

Wong, Man Long & Lele, Sanjiva K. 2017 High-order localized dissipation weighted compact nonlinear scheme for shock- and interface-capturing in compressible flows. *Journal of Computational Physics* **339**, 179 – 209.

Yamaleev, Nail K. & Carpenter, Mark H. 2009 A systematic methodology for constructing high-order energy stable WENO schemes. *Journal of Computational Physics* **228** (11), 4248 – 4272.

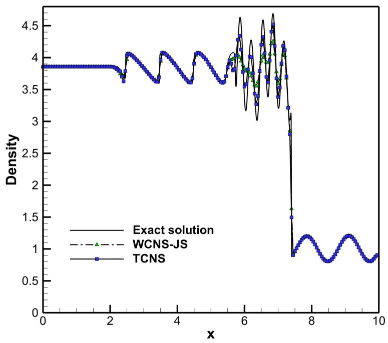

(a)

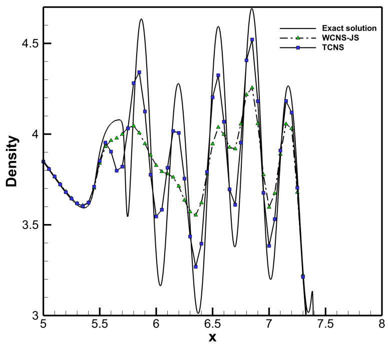

(b)

Figure 3. Shock-density wave interaction problem: numerical solutions and the exact solution at $t = 1.8$.

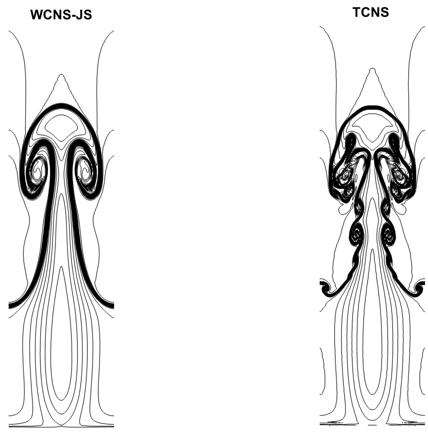

(a)

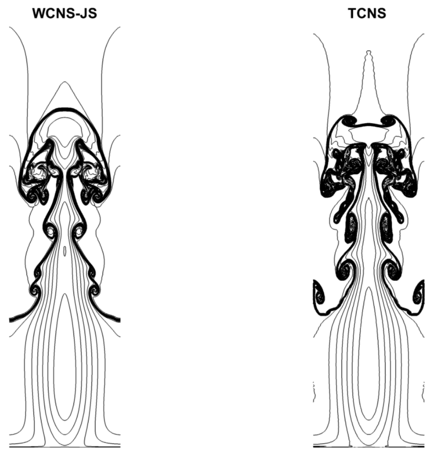

(b)

Figure 4. Rayleigh-Taylor instability problem: 30 density contour lines ranging from 0.9 to 2.2.